Materials Chemistry and Physics 293 (2023) 126898

Contents lists available at ScienceDirect

Materials Chemistry and Physics

journal homepage: www.elsevier.com/locate/matchemphys

Improved Difenoconazole pesticide detection limit via double-sided porous silicon layers' electrical sensor

Rasha B. Rashid, Alwan M. Alwan *, Mohammed S. Mohammed

Department of Applied Sciences, University of Technology, Iraq

HIGHLIGHTS

- Large surface area double-sided porous silicon was obtained by a novel etching process.
- Single and double-sided room temperature electrical sensors were fabricated.
- Large sensitivity and lower detection limit to trace Difenoconazole level is due to high adsorption rate.
- New electrical sensors involve parallel configuration of double-sided porous silicon layers.
- Present stable and an accurate sensor is based on external impedance matching RLC circuit.

GRAPHICAL ABSTRACT

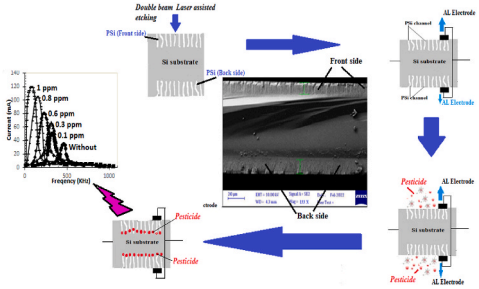

ARTICLE INFO

Keywords:
Porous silicon
Double sided
Morphologies
Electrical sensor
Pesticides

ABSTRACT

In this novel work, high-performance laser synthesized double-sided parallel porous silicon layers (Ds-Psi) pesticide sensors were employed. The Ds-Psi layers were synthesized via double beam laser-assisted etching (D-LAE). An easy run, cost-effective and non-poisonous process was adopted to investigate the Ds-Psi sensor performance. This process depended on recording the resonance frequency shift when exposing the pesticides to the sensor's surface. Two configurations were adopted: single-sided Psi sensor of Al/Psi/n c-Si/Al and parallel connected Ds- Psi layer of Al/Psi/c-Si/Psi/Al were synthesized and studied. Under ultra-low concentrations of Difenoconazole pesticide at room temperature, the current-frequency properties of the sensors revealed an excellent response of the Ds-Psi sensor compared with the single-sided Psi sensor. The results of the Ds-Psi sensor showed a much higher sensitivity (82.9%) and a lower detection limit of detection 0.001 ppm. The principal reason for this high performance is effectively related to the high surface area and large capacitance of the parallel configuration of the Ds-Psi layers. The synthesized impedance matching of the parallel configuration is very suitable for quantitative sensing of pesticides.

1. Introduction

Pesticides are sensed mainly through the use of sensors due to their increased presence in water and agricultural products as pollutants [1, 2]. Difenoconazole is one of the most important and widely insecticides used on fruits and vegetables. It has negative effects and complications and is classified as highly toxic substance dangerous to human health [3–5]; even at reduced concentrations (parts per billion) [6,7]. For food

* Corresponding author.
E-mail addresses: r1985asha@gmail.com (R.B. Rashid), alkrzsm@yahoo.com (A.M. Alwan), 100113@uotechnology.edu (M.S. Mohammed).

https://doi.org/10.1016/j.matchemphys.2022.126898
Received 11 August 2022; Received in revised form 26 September 2022; Accepted 10 October 2022
Available online 12 October 2022

safety and control applications, environmental pollution and health care, it is necessary to design sensors that are highly sensitive, stable and operate at room temperature [8]. Porous silicon (Psi) layers have received very wide interest in chemical sensing applications due to their very large surface area and easily modified microstructure [9–11]. The electrical resistance, capacitance and refractive index of the Psi layer may change appreciably when molecules are adsorbed to their surface [12]. The sensing performance of the Psi is varied according to the density of pores, muds, and pillars within the synthesized [13–15] structure. As this density increases, the sensitivity enhance rapidly. So to improve the possibility of sensing lower pesticide concentrations, the density of pores and pillars must be very high over the sensor surface [16]. The adsorption rate of porous layer is varied according to the specific surface area of the formed layer. The fabrication of single sided Psi layer was typically done with one side etching either by anodization or laser-assisted etching [17,18]. The Ds-Psi layer ensures higher surface area. The double side porous layer increases the total sensing area (area summation of both sides) whereas the specific surface area of each porous silicon layer does not change. This type of Psi structure was first synthesized by D. James et al. [19], by using an electrochemical etching cell with double tank configuration. P. Granitzer et al. [20], have prepared Ds-Psi layer of meso-structure embedded with metallic nanoparticles to improve the reflectance of the formed layer. The main target of this novel work is to synthesize a double sided PSi layer by double beam laser assisted etching pathway, and then using few of them in series to fabricate ultra-sensitive electrical sensor for detecting ultra-low Difenoconazole.

2. Experimental work

2.1. Ds-Psi layer synthesis

Low resistivity (0.01 Ω cm), n-type, mirror like surface, 500 μm thick silicon substrate and (100) orientation was employed to synthesize (Ds-Psi) samples by using double beam laser-assisted etching pathway (D-LAE). The Si substrate was cut into small pieces of (2 × 2) cm^2. These samples were washed with a dilute 10% HF acid for 10min to remove the native oxide layer and then rinsed with ethanol for 5 min and left in the air for a few minutes to dry and finally placed in a plastic container; filled with deionized water, to prevent the formation of an oxide film on the surface [21]. The (D-LAE) etching pathway was accomplished by utilizing a Teflon cell comprised of two transparent windows to illuminate both faces of Si substrate simultaneously. The etching process was carried out in a mixture of (HF: Ethanol) (1:1) for 10 min; where the HF concentration and the current density used were: 40% and 35 mA/cm^2 respectively. Two laser beams from a diode laser operating at 530 nm and 100 mW/cm^2 power densities were defocused in a circular spot of 1 cm diameter on both Si faces. The cathode was assembled from two platinum rings while the middle point contact of Si acted as an anode to complete the etching cycle.

2.2. Metallization of Ds-Psi layers

To accomplish metalizing the sensor, thick aluminum electrodes were thermally deposited on each porous silicon layers as shown in figure (2a) (see Fig. 1). The 3mm × 3 mm aluminum electrodes were thermally deposited in a way that it coats most of the porous layer area to reduce the surface leaking current. The position of both electrodes permitted the formation of Ds-Psi sensor with parallel configuration as Al/Psi/c-Si/p-Si/Al. On the other hand, the single sided Psi sensor was constructed by depositing two Aluminum layers on the front of Psi layer and on the back of the Si surface in a configuration symbolized as Al/Psi/c-Si/Al; as shown in Figure (2b). The sensing set up is shown in figure (2c). In Fig (2a), the resistance of the base Si substrate was neglected due to the low resistivity of silicon wafer. In this case, the equivalent electric circuit represents two junctions connected in parallel (one between the upper Psi layer and crystalline bulk silicon and the other between the bulk silicon and the lower Psi layer), as shown in figure (2d).

The sensing mechanisms of the current-frequency (I-f) characteristics were based on recording the resonance frequency shift after exposing the sensor to a pesticide solution. The (I-f) characteristics of a simple impedance matching electrical resistance-inductance-capacitance (R-L-C) circuit after exposure to concentrations from 0.01 to 0.1 ppm were measured at room temperature. The R-L-C circuit, figure (2c) consists of an external coil, Psi sensor, and a function generator at a frequency range (1 KHz to 1 MHz) in order to test the performance of the fabricated sensor in the absence and presence of Difenoconazole molecules. The 30 μH air coil was assembled from 18 turn, 80 cm^2 cross-sectional area and 3 mm diameter copper wire (to ensure a very low resistance). The AC applied voltage of the R-L-C circuit was fixed at 10 mV and the circuit was connected in series. After each measurement, the Psi sensor was cleaned by de-ionized water and dried with nitrogen gas. The sensor response depends essentially on the dielectric constant of the Difenoconazole solution, the possibility of filling the layer, the structures of the sensor, and the area per unit volume of the sensor. A specific weight of Difenoconazole was dissolved in methanol to prepare the required concentrations and each read-out was performed after 90 s of exposure duration to the pesticide solution. The resonance frequency measurement in the impedance matching circuit was obtained using hp33120a high precision function generator and 8846AFluke 6–1/2 Digit precision multimeter. The sensitivity S% is given by the ratio of resonance

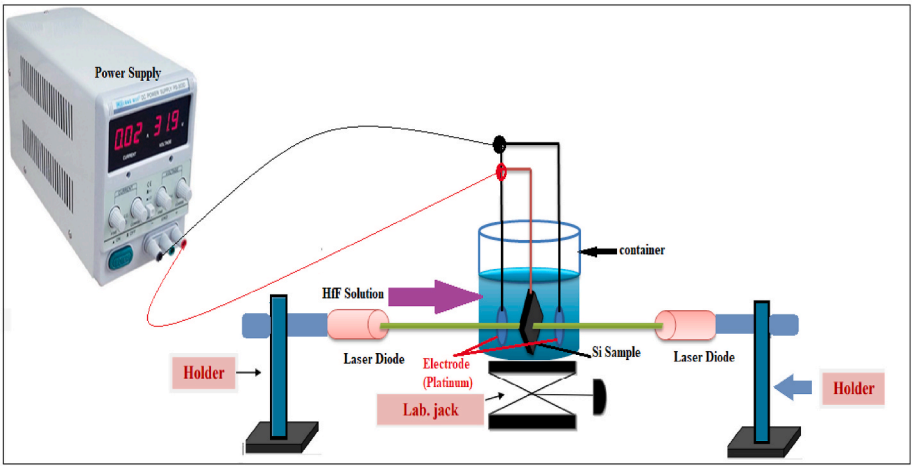

Fig. 1. Presents a schematic representation of the (D-LAE) experimental setup.

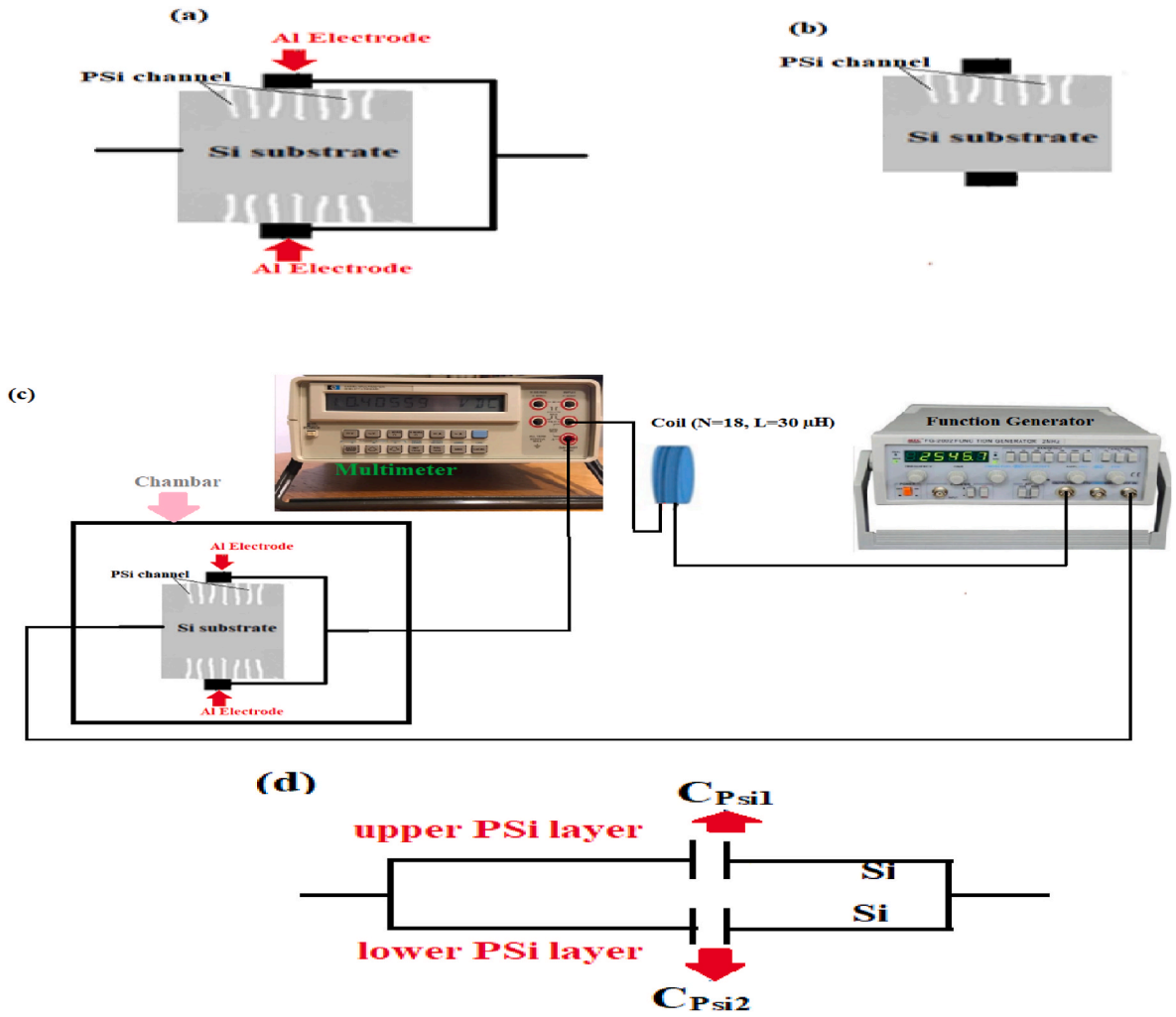

Fig. 2. The schematic representation of a) two sides, b) one side pesticide sensor configuration measurements and c) R-L-C circuit measurements set-up, d) equivalent circuit.

frequency shift Δf after exposure, to the resonance frequency f_o before the exposure as expressed in formula (1) [22].

$$S\% = \Delta f / f_0 \quad (1)$$

The sensor's ability to detect the smallest concentration of target molecules is called the limit of detection LOD and is given by equation (2); [23].

$$LOD = 3SD/slope \quad (2)$$

where; SD is the standard deviation, and the slope is taken from the plot between sensitivity and the Difenoconazole concentration. The morphological properties of one side and Ds-Psi were investigated using (ZEISS) field–Emission scanning electron microscope FE-SEM. The optical properties of the synthesized layer were also investigated using a continuous 320 nm, 500 mW He–Cd laser Horiba Jobin–Yovin T64000 PL spectrometer.

3. Results and discussion

3.1. Morphological features

The porosity of the synthesized layer was calculated by gravimetric method [9], while layer thickness, surface and cross sectional features of the synthesized layer were investigated by analyzing the cross sectional FE-SEM image after taking into account the scale bare of the FE-SEM micro-image. Porosity and thickness of the layer were (76%) and (18 μm) respectively. The surface morphology for both sides was a mud-like structure, consisted of isolated and interconnected mud regions separated by vertical trenches. Fig. 3, shows the surface morphology of the of Psi layer. It represents a complex combination of pillars-like and mud-like structures, and appears as a double-folded morphology. Each mud region consists of ultra-fine pillars' structures. These pillars are randomly distributed over the surface and extend vertically on the porous surface. The density of pillars and pores in porous surface is around (1×10^{11} pillars/cm^2) and ($7*10^{110}$ pores/cm^2). The histograms of pillars and pores dimensions are shown in Fig. 4 (a and b), with pillars dimensions in the range 30 nm–190 nm and average apex dimensions of 60 nm. The diameter of pores is between 45 nm and 220 nm with an average pores diameter of 130 nm. The creation of these specific morphologies could have been realized due to the resistivity decrease of the Si substrate. The etching process was accomplished in vertical manner; deeply inside rather than on the substrate surface. The spatial variation of laser power density across the beam diameter due to the Gaussian distribution during the etching pathway can modify the Si dissolution route during etching and leads to a complex network of muds, pores and pillars structures. The formation mechanism behind these results can be understood by referring to K. Cheah model [24,25].

The etching pathway depends on the rate of photo-generated electron-hole couples; where this rate is modified with the spatial distribution of the laser power density. Fig. 5(a–c), shows the cross sectional

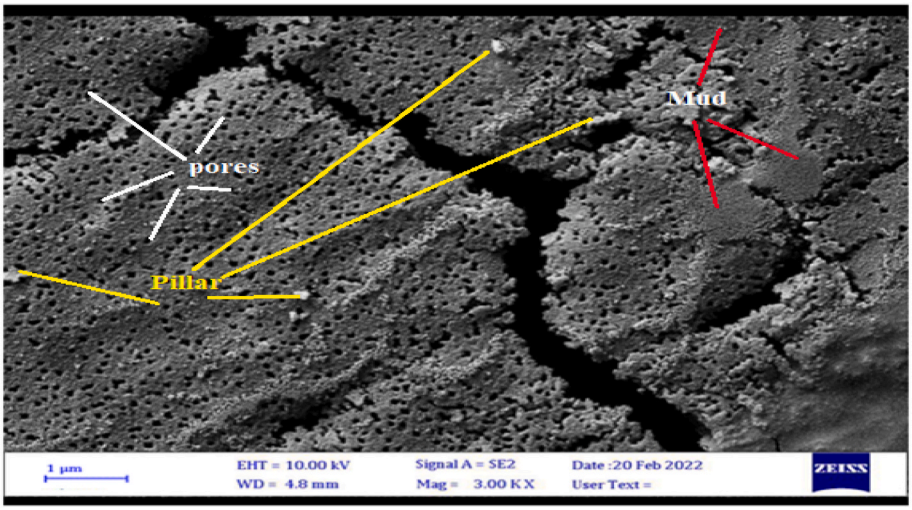

Fig. 3. Illustrates the FE-SEM images of surface morphology of upper and lower Psi layer.

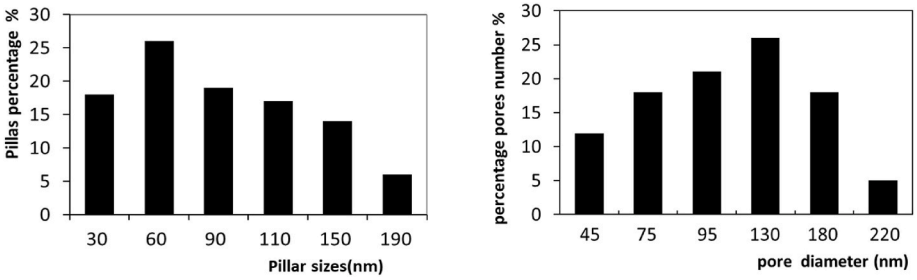

Fig. 4. Shows the histogram of a) pillars sizes, ands b) pores diameter in Psi layer.

image of the upper and lower Psi layers across the silicon substrate. This image illustrates, the morphology of Ds-Psi in which the silicon region is located between the upper and lower Psi layer layers. This figure clearly shows that the layer thickness of the upper side is slightly greater than the layer thickness of the lower side.

The photoluminescence PL spectra of the formed upper and lower PSi layer are illustrated in Fig. 6 (a, and b). For each layer, two distinguishable PL peaks of the emitted wavelengths are seen. For upper layer, the peaks are 640 and 669 nm corresponding to two energy gaps: (1.94 and 1.86) eV respectively. Also; for the lower layer, peaks emission wavelengths are 660 nm and 684 nm corresponding to the two energy band gap 1.88 eV and 1.82 eV. The presence of double PL peaks is a specific feature for double morphology (pores and pillar-like structures) with two silicon nanocrystallites size distributions. This explanation is in very good agreement with the quantum confinement model of electrically charged carriers within the matrix of the Psi layer. The PL intensity is strongly related to the amount of silicon nanocrystallites within the matrix whereas the peak emission wavelength is related to the dimensions of the Si nanocrystallites [26–28]. The emission peaks wavelength is strongly related to the etching laser wavelength and the power density. The application of short laser wavelength 530 nm and a high power density ≈100 mW/cm^2 can enhance the Si dissolution process within the formed layer and this, in turn, will increase the probability of existing silicon nanocrystallites with very small dimensions. The cumulative PL peak intensity is strongly connected with the density of nanocrystallites' luminescence in the formed layer due to the increase of the electron-hole recombination rate within the porous layer. The dependence of energy band gap (Eg) of porous silicon on the confinement dimensions was in good agreement with Suemune et al. model as expressed hereunder (3) [28].

$$\mathbf{Eg} = (\mathbf{Si}) + \frac{(\mathbf{h}^2\boldsymbol{\pi}^2\mathbf{D})}{(\mathbf{2mr}^*\mathbf{L}^2)} \tag{3}$$

where; mr* is the reduced effective mass, D is a constant equals 2 for a quantum pillar and 3 for silicon quantum dots, and L presents the confinement dimension. From the PL spectra, there is a little variation in energy band gap of Psi layers. This is related to the fluctuations of etching current density during the etching route. This fluctuation is established as a result of the resistance variation of the etching path between the platinum ring and the substrate.

3.2. *Electrical properties of parallel configuration Ds-Psi and one side Psi sensors*

The sensing principle of the fabricated sensors depends on monitoring the variations of dielectric constant of the one side Psi and Ds-Psi sensors, and hence; the electrical capacitance of the sensor after inserting the Difenoconazole molecules in the fabricated sensors. The variation of electrical capacitance can vary the resonance frequency in the impedance matching circuit. Fig. 7 (a,b), demonstrate the (I-f) characteristics of one side Psi sensor of configuration Al/Psi/n c-Si/Al and Ds-Psi sensor of parallel configuration Al/Psi/n c-Si/Psi/Al.

Fig. 7 shows that at the resonance frequency, the current in the impedance matching circuit reaches a peak value. As shown in Fig. (7a), when the one side Psi sensor was tested in the absence of the Difenoconazole at room temperature, the resonance frequency obtained was around 830 kHz corresponding to the highest value of current. In figure (7b) for the Ds-Psi with parallel configuration sensor, the resonance frequency is around 460 KHz. For both sensors, a very low Difenoconazole concentration of about (0.01 ppm) was exposed to sensors. An

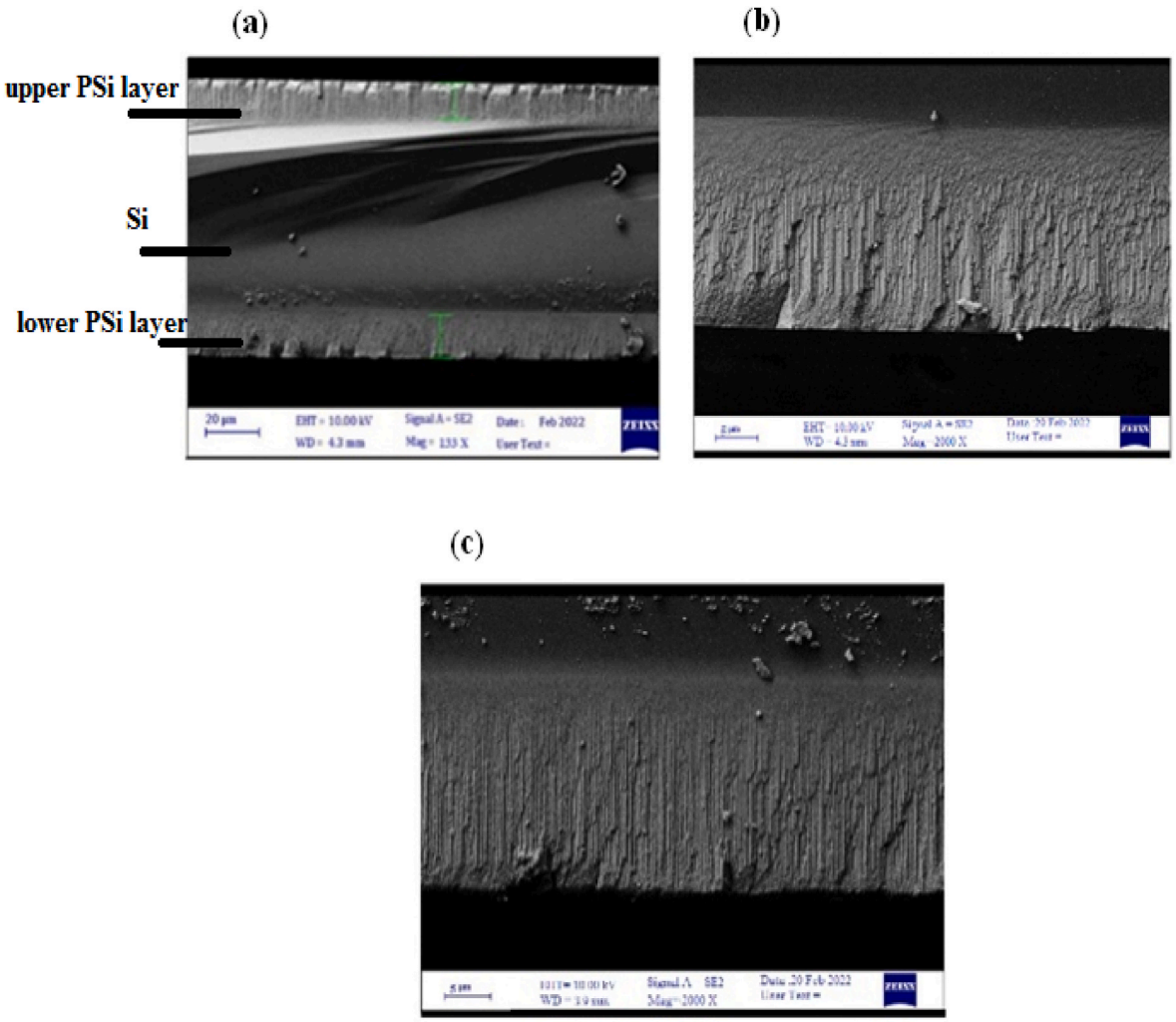

Fig. 5. Illustrates the cross sectional FE-SEM image of a) Ds-Psi layer, b) upper Psi layer, and c) lower Psi layer.

ultra-response especially for Ds-Psi sensor was achieved in the form of red resonance frequency shift. The new values of resonance frequency for the one side Psi sensor and the Ds-Psi sensor are about (770 KHz) and (325 KHz) respectively.

As the concentration of Difenoconazole increased to 0.1 ppm, the resonance frequency shifting to much lower frequencies reaching a minimum resonance frequency of about (610 KHz) and (180 KHz) for the one side and Ds-Psi sensors respectively. In Fig. 7, the current passing within the Ds-Psi sensor is higher than that of one side and the increase in the current after exposure to the Difenoconazole is strongly related to the density of vertical pillars and pores in the porous layer and an effective dielectric constant of Psi layer is shown in the following equation (4) [29].

$$\mathbf{J_{pSi}} = \boldsymbol{\varepsilon}_{\mathbf{r\ pSi}}\boldsymbol{\varepsilon}_{\circ}\boldsymbol{\mu}_{\mathbf{eff}}\frac{\mathbf{V^2}}{d^3} \tag{4}$$

Where ε_{rpsi} is a dielectric constant of psi, ε_o dielectric constant of air, μeff is the mobility of the charge carriers, V is the applied voltage and d is the Psi thickness. As a result of loading pesticide molecules within the Psi, the effective dielectric constant of the Psi is modified as shown in equation (5) [30]. For the Ds-Psi sensor in parallel configuration the total capacitance of the sensor is greater than the one side Psi sensor, which is a summation of capacitance of both sides, as given by equation (6). The output signal from the Ds-Psi is the contribution from both sides. This behavior is equivalent to effect of increasing of the surface area of the sensor. The circuit current is related to the rate of adsorption of Difenoconazole molecules, so it is increased with increasing the specific surface area of Psi [31]. These parameters in Ds-Psi are much higher than that of one side Psi. Therefore, the current in Ds-Psi is greater than that of one side Psi sensor [32].

$$\boldsymbol{\varepsilon}_{\mathbf{rpSi}} = \boldsymbol{\varepsilon}_{\mathbf{rSi}} - \mathbf{P}\%\left(\boldsymbol{\varepsilon}_{\mathbf{rSi}} - \boldsymbol{\varepsilon}_{\mathbf{rpore}}\right) \tag{5}$$

$$\boldsymbol{C}_{\boldsymbol{Total\ PSi}} = \boldsymbol{C}_{\boldsymbol{PSi1}} + \boldsymbol{C}_{\boldsymbol{PSi2}} \tag{6}$$

Fig. 8, presents the dependence of resonant frequency (f) on Difenoconazole concentrations in the range from 0.01 to 0.1 ppm for both sensors. This figure clearly shows that the resonance frequency of both sensors decreases in a semi-linear form with the Difenoconazole concentration; with a resonance frequency in Ds-Psi sensor lower than the one side due to the higher layer capacitance. The resonance frequency (f) is related to the capacitance c Psi of the sensor and the inductance of the external coil (L) and expressed in equation (7) [33].

$$\boldsymbol{f}_{\boldsymbol{resonance}} = \frac{\mathbf{1}}{\boldsymbol{2\pi\sqrt{LC_{PSi}}}} \tag{7}$$

The resonance frequency rise with concentration is attributed to the possibility of interaction between the sensor and the Difenoconazole molecules. This may in a way modify the dielectric constant efficiently. The responses of the sensors as a function of the Difenoconazole concentrations are represented as the slope of Fig. 8. Higher response (328.6 kHz/ppm) was achieved with Ds-Psi compared with (157) KHz/ppm from the one side sensor.

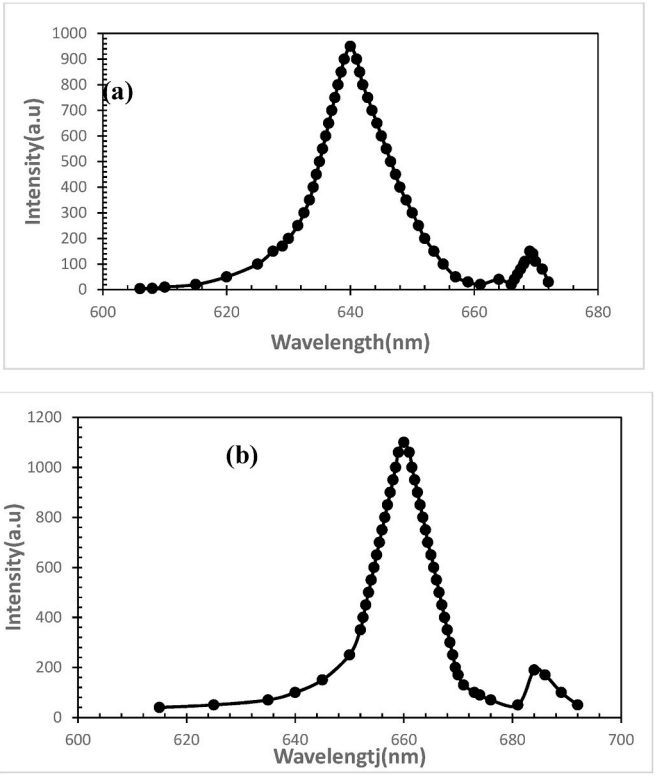

Fig. 6. The PL emission spectra of (a) upper side, and (b) lower side of Psi layer.

The significant parameter of the sensor's performance is its sensitivity which determines the ability of the sensor to respond to the pesticide molecules. The sensitivity was calculated using equation (1). The high sensitivity arises from its larger surface area that can adsorb a large amount of targets' molecules. The high sensitivity of the Ds-Psi sensor towards an ultra-low concentration as compared with one side is strongly related to the specific surface area in addition to the capacitance of the formed capacitor. The measured experimental values of the Psi sensor with air-filled matrix for one, and Ds-Psi, are 2.7 nF, and 5.1 nF correspondingly. Fig. 9 revealed the sensitivity of Psi to low concentrations of Difenoconazole at room temperature. This figure shows an increase in sensitivity with concentration. For 0.1 ppm of Difenoconazole molecules, for the one and Ds-Psi sensors, the sensitivities were 27.7% and 82.98% respectively.

The value of LOD was computed and found to be 0.006 and 0.001 ppm for Difenoconazole in the one and the Ds-Psi sensors, respectively. Remarkably, the employment of Ds-Psi in the sensing process with impedance matching circuit made significant contributions in detecting pesticides as compared to published work elsewhere [34]. The Obtained LOD of the Ds-Psi sensor was lower than that measured by an optical method which employed the SERS technique [35,36]. To explore the aging effects on the performance of the fabricated sensors, for long-term operation, the sensitivity was measured repeatedly every five days during the 40 days at 1 ppm concentration of Difenoconazole. The test displayed a highly stable performance Psi, as shown in Fig. 10, where the dropping rate in sensitivity for Ds-Psi is much better (0.1%) than that of the one side Psi sensor (0.21%) per day, respectively.

As the natural oxidation rate increased, the reduction rate in sensitivity increased too. Thus; both sensors offer excellent stability due to their lower reduction rate which is strongly related to the effective exposure volume of Psi to the ambient atmosphere. Based on sensitivity, LOD and stability results, the Ds-Psi sensor is the best to adopt, due to higher sensitivity and lower LOD, for pesticide sensing. The current Ds-Psi sensor represents a potential possibility for enhanced sensitivity,

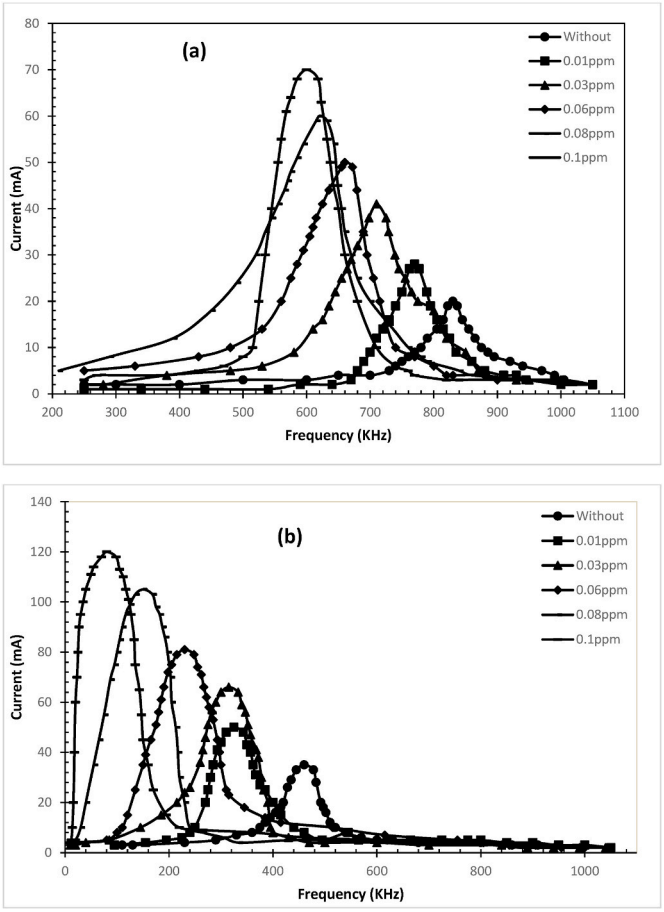

Fig. 7. Presents the current-frequency properties of a) one side and b) Ds_Psi sensors at concentrations from 0.01 ppm to 0.1 ppm.

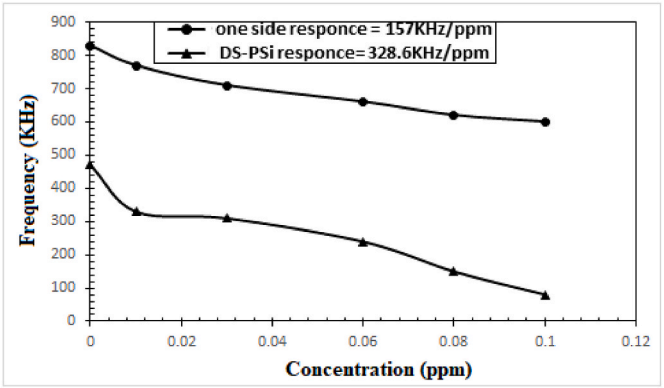

Fig. 8. Illustrates dependence of the resonant frequency of one side and Ds-Psi sensors at concentrations from 0.01 ppm to 0.1 ppm.

linear performance, stability, and low-cost design solutions.

4. Conclusion

This novel work successfully fabricated ultra-high sensitive impedance matching chemical sensors for detecting ultra-low pesticide concentrations. Laser synthesized double-sided porous silicon layers connected in the parallel configuration were employed to synthesize this sensor. Two electrical sensors: one and Ds-Psi layers with a sandwich top-bottom electrode configuration were synthesized and tested at room temperature. The Ds-Psi sensor with parallel configuration proved to be

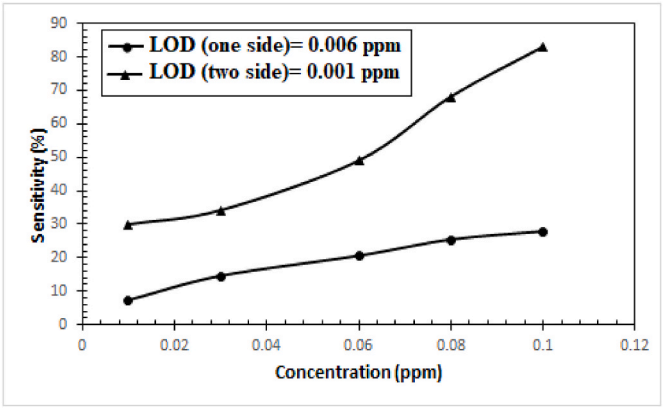

Fig. 9. Presents sensitivity of one and Ds_Psi sensors at concentrations from 0.01 ppm to 0.1 ppm.

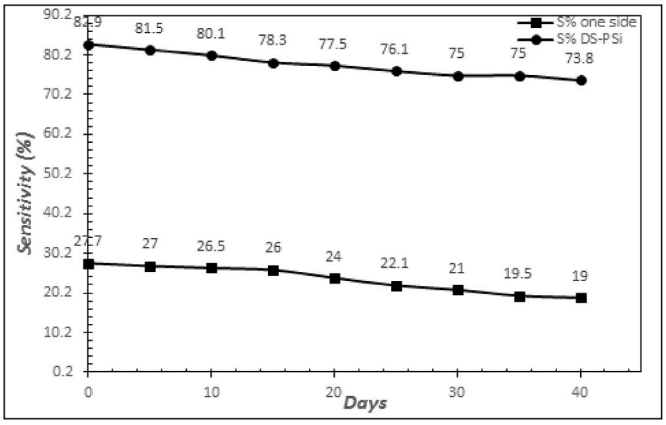

Fig. 10. Displays the dropping in sensitivity of one and Ds-Psi sensors at Difenoconazole concentration 0.1 ppm.

the best candidate for higher sensitivity and detection limit. The Ds-Psi layers can be employed as a potential choice for developing an efficient, low-cost, and simple operation sensor for the quantitative detection of chemicals.

Roles for authors

Rasha B. Rashid: Software, Visualization, Investigation. Alwan M. Alwan: Conceptualization, Methodology, Data curation, Writing- Original draft preparation, Supervision. **Mohammed S. Mohammed:** Validation, Writing- Reviewing and Editing, Supervision.

CRediT authorship contribution statement

Rasha B. Rashid: Software, Visualization, Investigation. **Alwan M. Alwan:** Conceptualization, Methodology, Data curation, Writing – original draft, Supervision. **Mohammed S. Mohammed:** Validation, Writing – review & editing, Supervision.

Declaration of competing interest

The authors declare that they have no known competing financial interests or personal relationships that could have appeared to influence the work reported in this paper.

Data availability

Data will be made available on request.

Acknowledgements

The authors would like to thank University of Technology (www.uotechnology.edu.iq) -Iraq, for your support in the present work.

References

[1] V.R. Pereira, D.R. Pereira, K.C. de Melo Tavares Vieira, V.P. Ribas, C.J. L. Constantino, P.A. Antunes, A.P.A. Favareto, Sperm quality of rats exposed to difenoconazole using classical parameters and surface-enhanced Raman scattering: classification performance by machine learning methods, Environ. Sci. Pollut. Res. 26 (2019) 35253–35265, https://doi.org/10.1007/s11356-019-06407-0.
[2] L. Hou, R.Y. Zhang, Z. Pang, S. Yang, T. Clark, J.M. He, Alteration of the non-systemic behavior of the pesticide ferbam on tea leaves by engineered gold nanoparticles, Environ. Sci. Technol. 50 (2016) 6216.
[3] L.A. Wali, K.K. Hasan, A.M. Alwan, Rapid and highly efficient detection of ultra-low concentration of penicillin G by gold nanoparticles/porous silicon SERS active substrate, Spectrochim. Acta Part A Mol. Biomol. Spectrosc. 206 (2019) 31–36, https://doi.org/10.1016/j.saa.2018.07.103.
[4] M. Arias-Estévez, E. López-Periago, E. Martínez-Carballo, J. Simal-Gándara, J. C. Mejuto, L. García-Río, The mobility and degradation of pesticides in soils and the pollution of groundwater resources, Agric. Ecosyst. Environ. 123 (2008) 247–260, https://doi.org/10.1016/J.AGEE.2007.07.011.
[5] A. Kalia, S.K. Gosal, Effect of pesticide application on soil microorganisms, Arch. Agron Soil Sci. 57 (2011) 569–596.
[6] S.J. Rowland, J.A.F. Rook, Analytical Methods, Int. J. Dairy Technol. 14 (1961) 112–114, https://doi.org/10.1111/j.1471-0307.1961.tb00962.x.
[7] L. Camenzuli, M. Scheringer, K. Hungerbühler, Local organochlorine pesticide concentrations in soil put into a global perspective, Environ. Pollut. 217 (2016) 11–18, https://doi.org/10.1016/j.envpol.2015.08.028.
[8] L. De Stefano, L. Moretti, I. Rendina, A.M. Rossi, Quantitative optical sensing in two-component mixtures using porous silicon microcavities, Phys. Status Solidi 201 (2004) 1011–1016.
[9] A.M. Alwan, A.J. Hayder, A.A. Jabbar, Study on morphological and structural properties of silver plating on laser etched silicon, Surf. Coating. Technol. 283 (2015) 22–28, https://doi.org/10.1016/j.surfcoat.2015.10.037.
[10] Canham, Silicon quantum wire array fabrication by electrochemical and chemical dissolution of wafers, Appl. Phys. Lett. 57 (1990) 1046–1104.
[11] X. Wang, E. Zhang, H. Shi, Y. Tao, X. Ren, Semiconductor-based surface enhanced Raman scattering (SERS): from active materials to performance improvement, Analyst 147 (7) (2022) 1257–1272, https://doi.org/10.1039/D1AN02165F.
[12] A.M. Alwan, R.B. Rashid, A.B. Dheyab, Morphological and electrical properties of gold nanoparticles/macroPorous silicon for CO2 gas, Iraqi J. Sci. 59 (2018) 57–66, https://doi.org/10.24996/IJS.2018.59.1A.8.
[13] P.R. Nair, M.A. Alam, Design considerations of silicon nanowire biosensors, IEEE Trans. Electron. Dev. 54 (2007) 3400–3408, https://doi.org/10.1109/TED.2007.909059.
[14] A.M. Alwan, Z.S. Ahmed, The opto-electronic characteristics of multi-porosity silicon system, Eng. Technol. J. 32 (2014).
[15] A.M. Alwan, A.A. Yousif, L.A. Wali, A study on the morphology of the silver nanoparticles deposited on the n-type porous silicon prepared under different illumination types, Plasmonics 13 (2018) 1191–1199, https://doi.org/10.1007/s11468-017-0620-3.
[16] A.B. Dheyab, A.M. Alwan, M.Q. Zayer, Optimizing of gold nanoparticles on porous silicon morphologies for a sensitive carbon monoxide gas sensor device, Plasmonics 14 (2019) 501–509, https://doi.org/10.1007/s11468-018-0828-x.
[17] R.B.R.c Alwan, M. Alwan a, R. Husam, b Abed, Enhancing the temporal response of modified porous silicon-based CO gas sensor, Solid State Electron. (2021) 181–182, https://doi.org/10.1016/j.sse.2021.108019, 50.
[18] F. Giorgis, E. Descrovi, A. Chiodoni, E. Froner, M. Scarpa, A. Venturello, F. Geobaldo, Porous silicon as efficient surface enhanced Raman scattering (SERS) substrate, Appl. Surf. Sci. 254 (2008) 7494–7497.
[19] T.D. James, A.J. Keating, G. Parish, L. Faraone, C.A. Musca, A technique for fabricating uniform double-sided porous silicon wafers, Electrochem. Solid State Lett. 10 (2007) D130.
[20] P. Granitzer, K. Rumpf, M. Albu, P. Pölt, Double-sided mesoporous silicon with embedded quasi-regular arranged ferromagnetic nanostructures fabricated by electrodeposition, ECS Trans. 25 (2010) 139.
[21] G. Foti, E. Rimini, S.U. Campisano, Laser annealing of Pb-implanted silicon, Phys. Status Solidi 47 (1978) 533–538.
[22] S.H. Wang, C.Y. Shen, J.M. Su, S.W. Chang, A room temperature nitric oxide gas sensor based on a copper-ion-doped polyaniline/tungsten oxide nanocomposite, Sensors 15 (2015) 7084–7095.
[23] L. Yande, Z. Yuxiang, W. Haiyang, Y. Bing, Detection of pesticides on navel orange skin by surface-enhanced Raman spectroscopy coupled with Ag nanostructures, Int. J. Agric. Biol. Eng. 9 (2016) 179–185.
[24] C.H. Choy, K.W. Cheah, Laser-induced etching of silicon, Appl. Phys. Mater. Sci. Process 61 (1995) 45–50, https://doi.org/10.1007/BF01538209.

[25] E.M. Abdelrazek, A.M. Alwan, M. Kamal, W.H. Ali, Investigation of Structural Properties of Gradient-Porosity Porous Silicon Layer Produced by Laser-Assisted Etching, 2014.
[26] I. Sychugov, R. Juhasz, J. Linnros, J. Valenta, Luminescence blinking of a Si quantum dot in a Si O 2 shell, Phys. Rev. B 71 (2005), 115331.
[27] S.H. Xu, Z.H. Xiong, L.L. Gu, Y. Liu, X.M. Ding, J. Zi, X.Y. Hou, Photon confinement in one-dimensional photonic quantum-well structures of nanoporous silicon, Solid State Commun. 126 (2003) 125–128.
[28] A. Hashimoto, K. Iwata, M. Ohkubo, A. Yamamoto, New laser ablation phenomenon of the porous Si films by focused N2 pulse laser irradiation, J. Appl. Phys. 75 (1994) 5447–5449.
[29] M.Q. Zayer, A.M. Alwan, A.S. Ahmed, A.B. Dheyab, Accurate controlled deposition of silver nanoparticles on porous silicon by drifted ions in electrolytic solution, Curr. Appl. Phys. 19 (2019) 1024–1030, https://doi.org/10.1016/j.cap.2019.05.010.
[30] Z. Kang, C.H.A. Tsang, Z. Zhang, M. Zhang, N. Wong, J.A. Zapien, Y. Shan, S.-T. Lee, A polyoxometalate-assisted electrochemical method for silicon nanostructures preparation: from quantum dots to nanowires, J. Am. Chem. Soc. 129 (2007) 5326–5327.
[31] A.M. Alwan, Calculation of energy band gap of porous silicon based on the carrier transport mechanisms, Eng. Technol. 25 (2007) 1143–1148.
[32] T.C. Dao, T.Q.N. Luong, Fabrication of uniform arrays of silver nanoparticles on silicon by electrodeposition in ethanol solution and their use in SERS detection of difenoconazole pesticide, RSC Adv. 10 (2020) 40940–40947, https://doi.org/10.1039/d0ra08060h.
[33] J.A. Camara, Electrical Engineering Reference Manual, for the Electrical and Computer PE Exam, 2006. Ppi.
[34] H. Lin, J. Mock, D. Smith, T. Gao, M.J. Sailor, Surface-enhanced Raman scattering from silver-plated porous silicon, J. Phys. Chem. B 108 (2004) 11654–11659.
[35] J. Li, Q. Wang, J. Wang, M. Li, X. Zhang, L. Luan, P. Li, W. Xu, Quantitative SERS sensor based on self-assembled Au@Ag heterogeneous nanocuboids monolayer with high enhancement factor for practical quantitative detection, Anal. Bioanal. Chem. (2021), https://doi.org/10.1007/s00216-021-03366-9.
[36] S.E.J. Bell, N.M.S. Sirimuthu, Quantitative surface-enhanced Raman spectroscopy, Chem. Soc. Rev. 37 (2008) 1012–1024, https://doi.org/10.1039/b705965p.